Received: 6 April 2021 | Revised: 6 December 2021 | Accepted: 27 January 2022

DOI: 10.1002/jnr.25028

RESEARCH ARTICLE

JOURNAL OF Neuroscience Research

Coupling of brain activity and structural network in multiple sclerosis: A graph frequency analysis study

Chenfei Ye[1] | **Jing Huang**[2,3] | **Li Liang**[4] | **Zehong Yan**[4] | **Zhigang Qi**[2,3] | **Xiong Kang**[2,3] | **Zheng Liu**[5] | **Huiqing Dong**[5] | **Haiyan Lv**[6] | **Ting Ma**[1,4,7,8] | **Jie Lu**[2,3]

[1]Peng Cheng Laboratory, Shenzhen, China

[2]Department of Radiology and Nuclear Medicine, Xuanwu Hospital, Capital Medical University, Beijing, China

[3]Beijing Key Laboratory of Magnetic Resonance Imaging and Brain Informatics, Capital Medical University, Beijing, China

[4]Department of Electronic and Information Engineering, Harbin Institute of Technology at Shenzhen, Shenzhen, China

[5]Department of Neurology, Xuanwu Hospital, Capital Medical University, Beijing, China

[6]Mindsgo Life Science Shenzhen Co. Ltd, Shenzhen, China

[7]Advanced Innovation Center for Human Brain Protection, Capital Medical University, Beijing, China

[8]National Clinical Research Center for Geriatric Disorders, Xuanwu Hospital Capital Medical University, Beijing, China

Correspondence
Ting Ma, Department of Electronics and Information, Harbin Institute of Technology at Shenzhen, Rm 1206, Information Building, HIT Campus, Shenzhen University Town Nanshan District, Shenzhen, 518055, Guangdong Province, China.
Email: tma@hit.edu.cn

Funding information
This study is supported by grants from the National Key Research and Development Program of China (2018YFC1312000), National Natural Science Foundation of P.R. China (81522021); the Beijing Municipal Administration of Hospitals "Dengfeng" Talent Training Plan (DFL20180802); the Beijing Municipal Science & Technology Commission (Z171100000117001), the China Postdoctoral Science Foundation funded project (2021M691686) and the National Natural Science Foundation of China (62106113)

Abstract

The brain activities and the underlying wiring diagrams are vulnerable in multiple sclerosis (MS). Also, it remains unknown whether the complex coupling between these functional and structural brain properties would be affected. To address this issue, we adopted graph frequency analysis to quantify the high-order structural-functional interactions based on a combination of brain diffusion and functional MRI data. The structural-functional decoupling index was proposed to measure how much brain regional functional activity with different graph frequency was organized atop the underlying wiring diagram in MS. The identified patterns in MS included (1) disruption of inherent structural-functional coupling in the somatomotor network ($\beta = 0.05$, $p = 0.03$), and (2) excessive decrease of decoupling in the subcortical ($\beta = -0.10$, $p = 0.02$), visual ($\beta = -0.04$, $p = 0.01$), and dorsal attention networks ($\beta = -0.12$, $p = 0.03$). Besides, this structural-functional coupling signature in the somatomotor network was associated with cognitive worsening of MS patients ($\beta = -24.31$, $p = 0.006$). Overall, our study unveiled a unique signature of brain structural-functional reorganization in MS.

KEYWORDS
brain structural network, clinically isolated syndrome, graph frequency analysis, multiple sclerosis, resting-state fMRI

Chenfei Ye and Jing Huang contributed equally to this work.

Ting Ma and Jie Lu share the corresponding authorship.

Edited by Cristina Antonella Ghiani and Elizabeth Johnson.Reviewed by Arzu Has and Hee Yeon Im.

1 | INTRODUCTION

Multiple sclerosis (MS) is acknowledged as an inflammatory neurodegenerative disorder affecting central nervous system with severe clinical manifestations (Filippi et al., 2018). Apart from the common brain hallmarks of MS such as demyelination and axonal loss (Zipp et al., 2013), an advanced understanding of brain structural network topology would further help illustrate the neuropathological substrate of MS progression and inform clinical intervention and prevention (Calabrese et al., 2015). Several diffusion MRI studies reported that the disruptions of brain structural connectivity (SC) network in MS patients, such as lower nodal connectivity (Charalambous et al., 2019; Solana et al., 2018), the reduced strength of rich-club connections (Shu et al., 2018), and increased network modularity (Tur et al., 2019). Meanwhile, recent neuroscientific investigations observed the contemporary presence of widespread reorganizations of brain functional activity in MS (Rocca et al., 2016; Tahedl et al., 2018). Aberrantly increased or decreased functional connectivity (FC) emerged on subcortical regions (i.e., the thalamus, amygdala, and basal ganglia) (Cui et al., 2017; Sbardella et al., 2017; Schoonheim et al., 2014) and the temporal gyrus (Bisecco et al., 2019; Liu et al., 2016) were suggested to exhibit both adaptive (preventing impairment) and maladaptive (worsening impairment) effects (Tahedl et al., 2018; Zhang et al., 2021). Together, evidences suggested that both brain structural network and functional activity played critical roles in MS-related deficits. However, it is still poorly understood how these two components affect each other in MS evolution and modulate clinical manifestation.

Given that functional activity is shaped by the underlying wiring diagram (Bassett & Sporns, 2017; Stiso & Bassett, 2018), it is essential to clarify the macroscopic interdependency degree between the brain functional activity and the structural network or better understanding of MS mechanism. Most multimodal MRI studies calculated SC-FC correlation coefficients to quantify the degree of brain structural-functional coupling (for review, see (Wang et al., 2015)). In early-stage MS, the dynamic altered brain SC-FC correlations were observed when predicting patients' cognitive function and clinical disability (Koubiyr et al., 2019, 2021). However, this direct SC-FC correlation was criticized as being oversimplified (Suarez et al., 2020). The relatively sparse SC could only explain less than 50% of the variance in FC (Honey et al., 2009), partly due to indirect signaling between neuronal populations via common neighbors in a complex network. Therefore, a comprehensive evaluation of high-order brain structural-functional coupling is necessary to gain insights into the MS neuropathological mechanism.

The recently developed approach, named graph frequency analysis (GFA) (Huang et al., 2016), opens an avenue to quantify high-order structural-functional interactions among brain regions. Briefly, the brain regional activity measured by fMRI signals could be separated into several portions in the graph domain corresponding to various connectome harmonics from low to high frequency (Atasoy et al., 2016, 2018). By calculating the energy ratio of the decoupling portion to the coupling portion, GFA allows us to quantitatively evaluate how much functional activity aligns with or deviates from the structural constraints in MS, and how this level relates to disease disabilities.

Significance

Based on the hypothesis that the brain structural-functional interplay would be disrupted by the progression of neuroimmune inflammation, we focused on quantitatively measuring the brain coupling signature between functional activities and structural connectome affected by clinically isolated syndrome and relapsing-remitting multiple sclerosis (MS). Our results demonstrated the abnormality of brain structural-functional coupling affected by MS progression was associated with cognitive function. The current findings suggest a unique signature of brain structural-functional reorganization in MS.

In this study, we aim to investigate the high-order brain structural-functional interaction related to MS using GFA. In particular, we recruited 55 MS patients, including 16 in clinically isolated syndrome (CIS) stage and 39 in relapsing-remitting MS (RRMS) stage, as well as 58 age-matched healthy controls (HCs). After first describing the basic characteristics of structural-functional coupling in HC, we extended GFA approach on the MS cohort to evaluate how much functional activity in MS aberrantly align with or deviate from the structural connectome at brain intrinsic connectivity network (ICN) level. Finally, we examined the relationship between brain structural-functional coupling and MS-related clinical phenotypes (disease severity and cognitive function).

2 | METHODS

2.1 | Study participants

This cross-sectional observational study recruited a total of 122 MS and HC participants from Xuanwu Hospital of Capital Medical University, Beijing, China. After removing eight subjects due to imaging quality control (see Figure S1), 16 CIS patients (mean age 30.2 ± 8.4, 6 females), 39 RRMS patients (mean age 34.0 ± 9.4, 14 females), along with 58 age-matched HCs (mean 32.2 ± 10.2, 18 females) were selected during 2016 to 2019. All of these participants were right handed measured by the Edinburgh Inventory to remove the potential handedness effects on diffusion measures (Tinelli et al., 2013). The CIS patients were prospectively examined with a clinical episode suggestive of MS within 6 months from onset (Miller et al., 2012). All MS patients presented with a relapse-remitting course and fulfilled the 2010 modified McDonald's criteria (Polman et al., 2011). To exclude the potential confounding effects of inflammation or edema on brain structure and function, all patients in the current study were in remission without relapse. None of the CIS

TABLE 1 Characteristics of participants

Characteristics	Mean ± *SD* [min–max]				*p* values (T or χ^2 statistic or W)			
	HC (*n* = 58)	MS (*n* = 55)	CIS (*n* = 16)	RRMS (*n* = 39)	HC vs. MS	HC vs. CIS	HC vs. RRMS	CIS vs. RRMS
Age (years)	32.2 ± 10.2 [20–59]	32.9 ± 9.2 [16–50]	30.2 ± 8.4 [17–44]	34.0 ± 9.4 [16–50]	0.7 (–0.4)[a]	0.7 (0.5)[a]	0.4 (–0.9)[a]	0.2 (–1.0)[a]
Sex (M:F)	40:18	35:20	10:6	25:14	0.7 (0.20)[b]	0.9 (0.04)[b]	0.8 (0.08)[b]	0.9 (0.01)[b]
Median disease duration (months)	NA	16 [0.5–252]	1 [0.5–6]	36 [1–252]	NA	NA	NA	<0.001 (–3.6)[a]
EDSS	NA	2.9 ± 1.5	2.0 ± 1.1	3.3 ± 1.5	NA	NA	NA	0.003 (–3.1)[a]
PASAT-2	NA	34.8 ± 9.1	41.1 ± 6.5	32.2 ± 8.75	NA	NA	NA	<0.001 (3.7)[a]
PASAT-3	NA	41.4 ± 8.4	48.8 ± 4.6	38.4 ± 7.7	NA	NA	NA	<0.001 (5.1)[a]
Median T2 - LV (mm^3)	NA	3,667 [0–60,228]	524 [0–35,288]	7,520 [188–126,108]	NA	NA	NA	0.03 (193)[c]

Abbreviations: CIS, clinically isolated syndrome; EDSS, expanded disability status scale; HC, healthy control; MS, multiple sclerosis; NA, not applicable; PASAT, paced auditory serial addition test; RRMS, relapsing-remitting multiple sclerosis; T2 - LV, T2 lesion volume.

[a]Independent two-sample *t* test.

[b]Chi-squared test.

[c]Wilcoxon rank-sum test.

and MS patients had been treated with medications (e.g., corticosteroids and disease-modifying medications) within 4 weeks before MRI scanning. Our study was approved by the Xuanwu Hospital Ethics Committee. Written informed consents were obtained from all participants.

2.2 | Clinical assessment

The demographic and clinical characteristics, including disease duration, Expanded Disability Status Scale (EDSS) score (Kurtzke, 1983), and 2-second and 3-second paced auditory serial addition tests (PASAT-2 and PASAT-3), were recorded by an experienced neurologist (H.D., with more than 25 years of experience in neurology) at the time of the MRI. These PASAT scales assessed patients' cognitive function, particularly in working memory, attention, and arithmetic capabilities. The demographic and clinical characteristics of all participants are demonstrated in Table 1.

2.3 | Imaging protocol

The MRI data were acquired on a 3.0 T MR system (Trio Tim; Siemens, Erlangen, Germany) with a 12-channel head coil. The following MRI sequences were performed: T1-weighted MRI protocol: magnetization-prepared rapid gradient-echo sequence, inversion time (TI) = 1,000 ms, echo time (TE) = 2.13 ms, repetition time (TR) = 1,600 ms, field of view (FOV) = 256 × 256 mm^2, isotropic voxel size = 1 mm, flip angle = 9; T2-weighted MRI protocol: turbo spin echo sequence, 35 axial slices, TE/TR = 87/5,000 ms, FOV = 256 × 256 mm^2, voxel size = 1 × 1 × 4 mm^3; diffusion MRI protocol: spin echo EPI sequence, TE/TR = 98/11,000 ms, FOV = 256 × 232 mm^2, flip angle = 90, isotropic voxel size = 2 mm, 60 gradient directions with b = 1,000/2,000 s/mm^2, and two additional b0 image; and resting-state functional MRI protocol: single-shot gradient-echo T2* with 180 dynamics, TE/TR = 30/2,000 ms, FOV = 220 × 220 mm^2, matrix = 64 × 64 × 32, slice thickness = 3 mm, acquisition time = 7 min. Additional T2-weighted sagittal scans on spinal cord were also acquired to examine focal lesions.

2.4 | Processing of MRI data

Lesion filling was performed ahead of brain anatomical parcellation to avoid potential spuriously segmented thinned cortex in MS patients (Tillema et al., 2016). In our practice, hyperintense white matter lesions were manually delineated on MS patient's T2-weighted images by an experienced neuroradiologist (Q. Z.) using MRIcro software (https://www.mccauslandcenter.sc.edu/crnl/mricro/). By T2-to-T1 rigid image coregistration using FSL-flirt 6.0, the obtained binary lesion masks were transformed and filled the T1-weighted image using *lesion_filling* command in FSL (Battaglini et al., 2012) for MS individuals. Then each individual T1-weighted

brain cortical surface was anatomically parcellated by FreeSurfer V6.0 pipeline (Fischl, 2012) and further converted to 360 cortical regions defined by Glasser's multimodal atlas by surface mapping (Glasser et al., 2016). For quality control, the cortical parcellations of one CIS and three RRMS patients were manually edited, according to the surface editing steps described in McCarthy et al. (2015). Specifically, we inserted control points around error regions for each hemisphere, and reran *autorecon2* in FreeSurfer pipeline to correct surface errors. To define individual subcortical regions, we also used FSL-FRIST pipeline to segment the thalamus, the hippocampus, the amygdala, the putamen, the caudate, the pallidum, the ventral diencephalon, the accumbens bilaterally, and the brainstem (Patenaude et al., 2011). We replaced the bilateral hippocampus defined in Glasser's multimodal atlas with the extracted volume by FSL-FIRST pipeline to achieve better parcellation accuracy. Finally, 375 brain cortical and subcortical parcel labels for each participant were obtained in native T1-weighted space.

Image preprocessing of diffusion MRI data, including denoising, motion correction, b0 and eddy current distortion correction, was performed by MRtrix 3.0.0 (Tournier et al., 2012). Then fractional anisotropy (FA) map was estimated based on diffusion tensor modeling to quantitatively measure the disruption of brain WM microstructure. Moreover, the diffusion-weighted images were applied to estimate the multi-shell fiber orientation distribution using constrained spherical deconvolution (Tournier et al., 2008) with a default maximum spherical harmonic degree $l_{max} = 8$. To improve the biological plausibility of the generated streamlines, we referred to the anatomical-constrained tractography method for tractography estimation (Smith et al., 2012). In our practice, both the brain segments (i.e., gray matter, white matter, and cerebrospinal fluid) based on high-resolution T1-weighted images and the lesion masks manually delineated on T2-weighted images were used to constrain streamline propagation. This strategy was adopted here for fiber tracking because certain white matter tracts including the optic radiation can be reconstructed with higher accuracy level compared with conventional strategies in MS patients (Horbruegger et al., 2019). The second-order Integration over Fiber Orientation Distributions (iFOD2) algorithm (Tournier et al., 2010) was applied to estimate 5 million probabilistic streamlines as follows: FOD amplitude threshold = 0.1, step size = half original voxel size, maximum curvature per step = 45°. We further performed the spherical-deconvolution informed filtering (SIFT) algorithm to obtain the tractogram containing 1 million streamlines to improve biological accuracy and reproducibility (Smith et al., 2015). By SyN (ANTs v2.1.0) nonlinear image coregistration (Avants et al., 2008) from b0 to native T1-weighted image, we used the inverse transform map to warp the brain parcel labels into the individual diffusion MRI space. From these tractogram and anatomical parcellations, the individual white matter structural network matrix $\boldsymbol{A}$ was constructed, where each element represented the number of streamlines connecting brain regions adjusted by streamline length (Hagmann et al., 2007).

The resting-state fMRI images were preprocessed by fMRIPrep 20.1.3 (Esteban et al., 2019). In brief, functional data were processed by slice timing correction using *3dTshift* from AFNI (Cox, 1996), motion correction using FSL-mcflirt (Jenkinson et al., 2002), and BOLD-to-T1w transformation using *bbregister* in FreeSurfer V6.0 with nine degrees of freedom (Greve & Fischl, 2009). These preliminary processing stages were then followed by the confound regression using *CompCor* and spatial smoothing with an isotropic 5 mm Gaussian kernel using xcpEngine (https://github.com/PennBBL/xcpEngine) (Ciric et al., 2017). The linear trend, mean framewise displacement measured by head motion Friston-24 model (Friston et al., 1996), and signals from white matter and cerebrospinal fluid were also regressed out as nuisance covariates. None of the participants was found with the mean displacement > 2.5 mm in quality check to assess head motion. By mapping the subject-specific anatomical parcellations defined in the corresponding high-resolution T1-weighted image via transformation matrix returned by *bbregister* procedure, the resultant *z*-scored BOLD signal averaged on each brain region was chosen as the brain functional activity measure. To further identify the corresponding relationship between each brain network node and ICNs, all cortical brain parcels in Glasser's multimodal atlas were mapped to the seven networks predefined by Yeo atlas in MNI space (Yeo et al., 2011). All the MRI images and parcellation results have been visually checked by an experienced neuroradiologist (J. H., with more than 10 years of experience in neuroradiology) and passed quality control. The network graph metrics including global efficiency, clustering coefficient, and modularity were further calculated using *bctpy* 0.5.2 tool (https://github.com/aestrivex/bctpy).

2.5 | Graph Fourier analysis theory

To explicitly characterize the brain structural-functional coupling, we applied GFA approach (Huang et al., 2016) to quantify the alignment or liberality extent of the brain activity with respect to the underlying structural network. Analogous to the classic Fourier transformation which decomposed time-domain signal into multiple frequency-domain bands, GFA enables us to empirically separate the functional activity (BOLD signals) on each graph node, timepoint by timepoint, into various harmonic components (Atasoy et al., 2018). Explicitly, the harmonic component with low frequency corresponds to the aligned brain activity along the geometrical network pathways, while the one with high frequency represents the rapidly varying brain activity with respect to the structural topological pattern. The computational pipeline of GFA is conceptually illustrated in Figure 1. Given an individual brain structural network matrix $\boldsymbol{A}$, we applied the eigenvector decomposition on the graph $L = V\Lambda V^T$ after a Laplacian shift $L = D - A$, where D denotes the diagonal degree matrix of $\boldsymbol{A}$. Following Huang's work (Huang et al., 2016), the derived eigenvalues λ_k with the order $\lambda_1 \leq \lambda_2 \leq \cdots \leq \lambda_n$ referred to graph frequencies from low to high level, while the corresponding eigenvector u_k can be interpretated as connectome harmonics (Atasoy et al., 2018). The graph Fourier transform of the brain BOLD signals

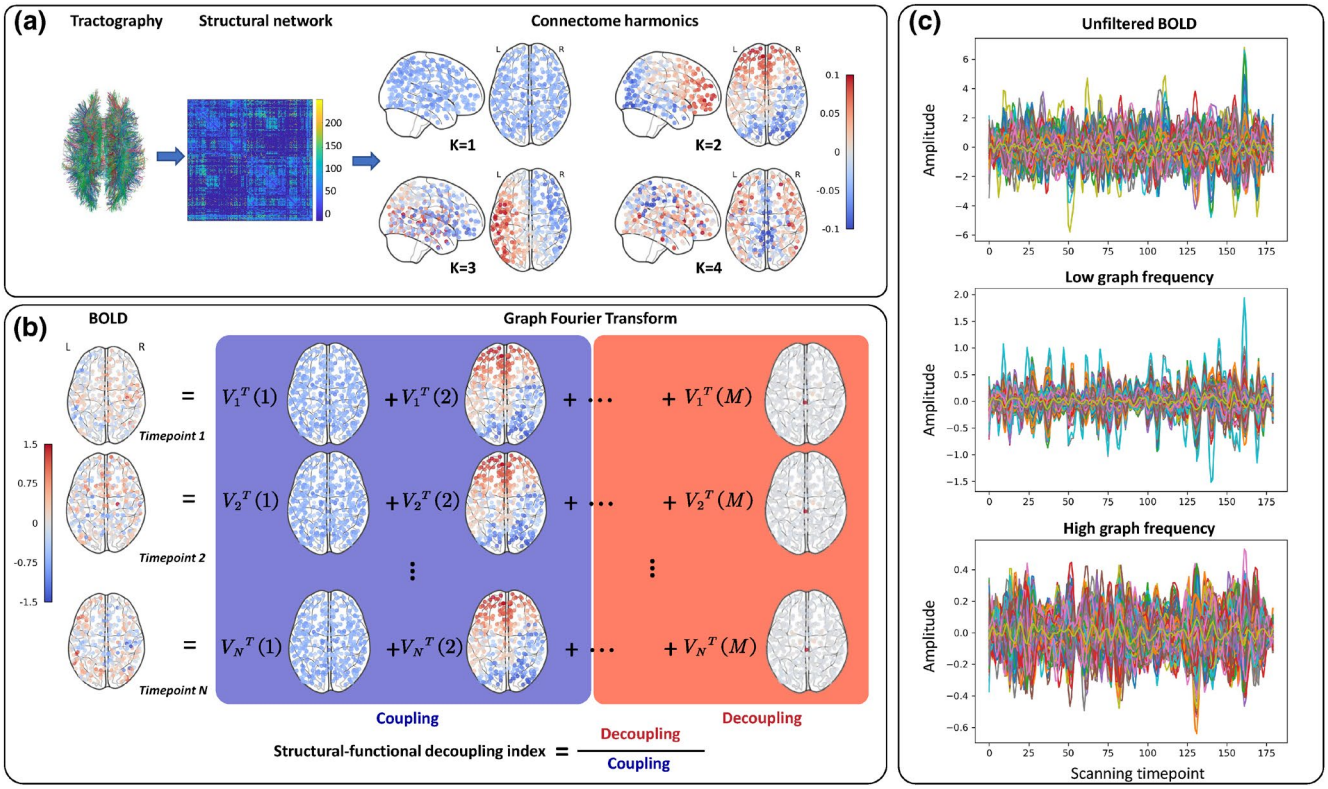

FIGURE 1 Schematic flowchart of the graph frequency analysis. (a) The individual brain structural network established by tractography on diffusion MRI data was transformed to separate connectome harmonics by graph Fourier transform. (b) The BOLD signals at every timepoint were further represented as a linear combination of connectome harmonics from low to high graph frequency (structural Laplacian eigenvalues). SFDI was calculated as the ratio between the high-frequency (decoupling) portion and the low-frequency (coupling) portion. (c) The unfiltered BOLD time series of 375 parcellated brain regions from a randomly selected participant (top), as well as the corresponding filtered BOLD signals associated with the lowest (middle) and highest (bottom) five frequencies

$x_t \in R^n$ in timepoint t with respect to Laplacian graph $\boldsymbol{L}$ was defined as:

$$\widetilde{x}_t = V^T x_t \tag{1}$$

Then the inverse graph Fourier transform of $\widetilde{x}_t$ is represented as:

$$x_t = V\widetilde{x}_t \tag{2}$$

Consequently, the graph Fourier transform coefficient $\widetilde{x}_t$ indicated the extent to which the observed brain functional activity deviates from the anatomical topology.

2.6 | Calculation of brain structural-functional decoupling index

Inspired by a previous study (Preti & Van De Ville, 2019), we applied the median-split strategy to filter the functional activity into low-frequency (alignment) and high-frequency (liberality) portions with equal energy:

$$x_t = x_t^{\text{low}} + x_t^{\text{high}} \tag{3}$$

To measure how much the local functional activation orients toward alignment or liberality with respect to the anatomical constraints, the *structural-functional decoupling index* (SFDI) was further introduced as the ratio between the norms of x_t^{low} and x_t^{high} across time. The higher value of SFDI represents liberality and the lower value represents alignment. We consider the mean SFDI value across the brain regions as a concentration measure of a specific ICN.

2.7 | Null model generation

To evaluate the robustness of SFDI, the spectral randomization method (Pirondini et al., 2016) was introduced to create surrogate brain functional signals based on the empirical structural network matrix *A*. Specifically, we randomly changed the sign of the graph spectral coefficients for 100 times to generate surrogate functional signals, as indicated below:

$$x_t^{\text{rand}} = VPV^T x_t \tag{4}$$

where $\boldsymbol{P}$ is a diagonal matrix with random +1/−1 values. The surrogate SFDI was further calculated based on the individual structural network matrix $\boldsymbol{A}$ and each surrogate functional activity x_t^{rand} to characterize

a null distribution. The coupling extent was determined to be significantly concentrated if the empirical SFDI among all participants was less than 95% of the null randomizations. This null model was deployed to assess whether the parcel-level or ICN-level properties of brain structural-functional interplay could be robustly maintained.

2.8 | Statistical analysis

To explore the potential network factors that account for ICN-level SFDI variations in HC, we calculated Spearman correlation to assess the ICN-level relationship between SFDI and the topological properties (described by graph metrics including the sum of connectivity strength, global efficiency, clustering coefficient and modularity, see (Sporns, 2011) for details). Then we applied general linear model (GLM) to evaluate MS versus HC group effect on ICN-level SFDI, adjusting age, sex, and head movement effects. For the assessment of imaging-behavior association, we investigated the relationship between the clinical phenotypes (i.e., EDSS, PASAT-2, and PASAT-3 scales) and SFDI by GLM for each ICN, after controlling for the same covariates. Overall, statistical analysis in current study was all performed using R (version 3.6.1, https://www.r-project.org/). Multiple group tests were controlled by false discovery rate (FDR) correction. Adjusted $p < 0.05$ or less was considered statistically significant.

3 | RESULTS

3.1 | Demographic and clinical information

Table 1 described the characteristics of the participants in the current study. No significant difference was observed in age ($T = -0.4$, $p = 0.7$) or sex distribution ($\chi^2 = -0.2$, $p = 0.7$) between MS and HC. RRMS had a longer disease course ($T = -3.6$, $p < 0.001$), worse disability ($T = -3.1$, $p < 0.001$ for EDSS scale), worse cognitive performance ($T = 3.7$, $p < 0.001$ for PASAT-2, $T = 5.1$, $p < 0.001$ for PASAT-3), and more lesion loads in brain ($W = 193$, $p = 0.03$ for T2 lesion volume, Wilcoxon rank-sum test) than CIS patients.

3.2 | Brain activity decomposition

The brain activity at each timepoint was decomposed into various connectome harmonics weighted by eigenvalues after graph Fourier transform, as illustrated in Figure 1. BOLD signal and the spatial patterns of the corresponding connectome harmonics were rendered based on group averaged values among HC. In congruent with the brain structural spectral patterns discovered by previous studies (Atasoy et al., 2016; Preti & Van De Ville 2019), one can observe that the connectome harmonics with low graph frequency maximally preserve global geometric distribution of the underlying anatomical topology (e.g., homogeneous across the brain for the first harmonic, anterior–posterior covarying for the second harmonic, and left–right covarying for the third harmonic) (Figure 1a), while those with high graph frequency encoded localized spatial patterns (Figure 1b). Notably, the brain activity was concentrated preferentially in lower frequency components, as shown in the BOLD power spectrum density curve (see Figure S2). To intuitively visualize the time-domain functional activity after graph decomposition, Figure 1c. showed the high and low graph frequency components of BOLD signals from all 375 brain parcels for a randomly selected healthy control. While the functional signals filtered by low pass connectome harmonics (corresponding to the lowest 5 graph eigenvalues) varied consistently and smoothly on all brain regions, the filtered signals with high graph frequency (corresponding to the highest five graph eigenvalues) illustrated high spatial variability with small amplitude.

3.3 | Brain regional coupling patterns

The human brain regional coupling pattern was illustrated by projecting HC group-average SFDI on brain network nodes (see Figure 2b). As for a spatial reference, Figure 2a demonstrated the node-ICN belonging relationship according to cortical Yeo atlas and parcellated subcortical regions, where each nodal color denotes the corresponding ICN. One can observe two main patterns emerged with excessive structural-functional coupling expression in Figure 2b. The former pattern located in frontal–parietal and subcortical area exhibited more structural-functional decoupling, whereas the latter coupling pattern concentrated in orbito-occipital areas. By the null model with randomized surrogate functional signals, we found six ICNs, including the visual, somatomotor, dorsal attention, frontoparietal, default, and subcortical networks, exhibiting significantly robust SFDI distribution in HC ($p < 0.001$ for each ICN, see Figure 3a). Interestingly, the mean value of SFDI on these ICNs largely diverged along a macroscale functional gradient (see Figure 3b), from unimodal ICN (e.g., the visual and somatomotor networks with structural-functional coupling) to transmodal ICN (e.g., the dorsal attention and frontoparietal networks with structural-functional decoupling).

3.4 | Factors affecting decoupling index variations in HC

First, none of age, sex, and head motion had any significant effect on ICN-level SFDI in HC (see Table S1). For FC network topology, none of the graph metrics (global efficiency, clustering coefficient, and network modularity) was correlated with SFDI in any ICN (see Table S2). For SC network topology, no ICN-level distribution similarity was observed between the sum of SC strength (see Figure S3) and SFDI in HC (see Figure 3). On the other hand, significant positive correlations were found in the default ($r = 0.38$, $p = 0.01$), dorsal attention ($r = 0.60$, $p < 0.001$), and frontoparietal

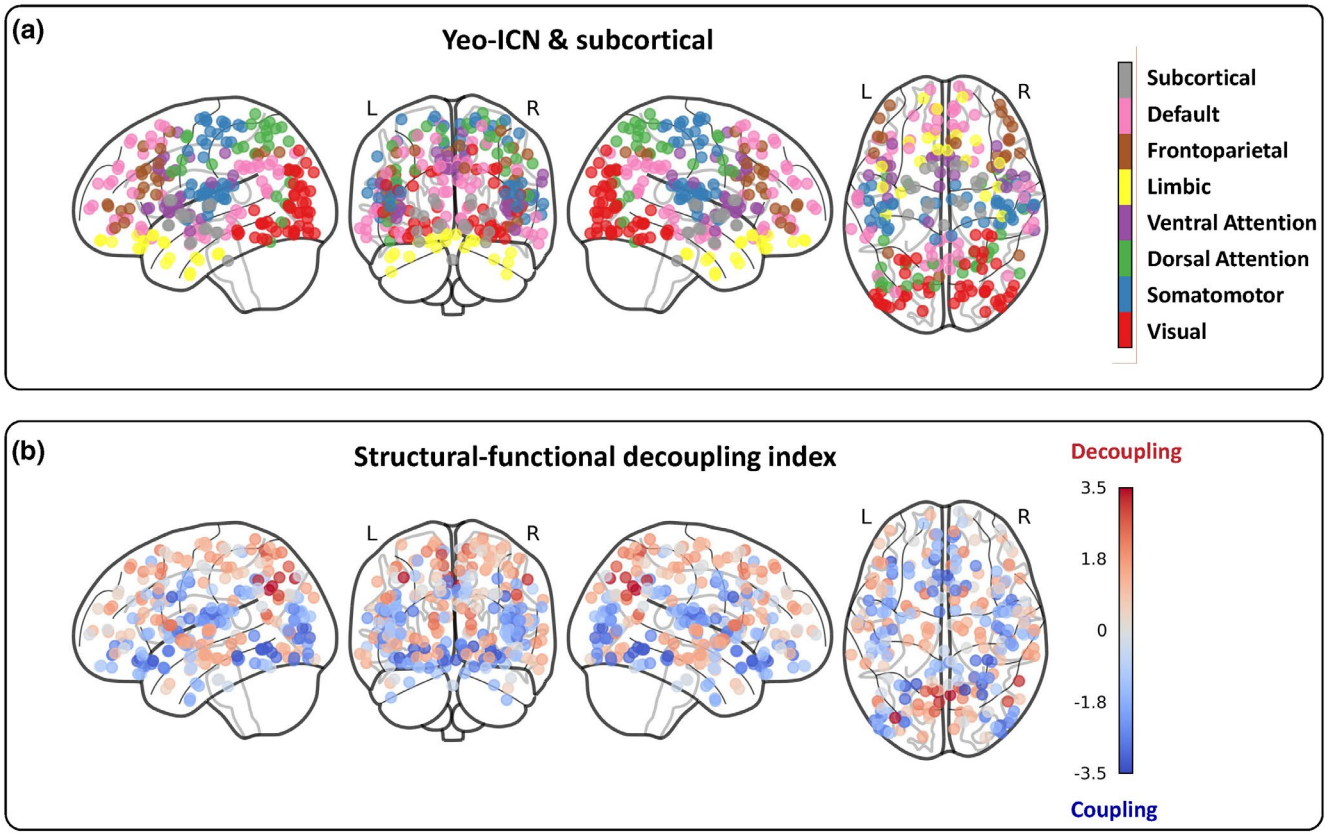

FIGURE 2 The mean SFDI of HC group projected on brain ICNs. (a) The parcellated brain regions belonging to the seven ICNs defined by Yeo atlas and subcortical network. (b) The mean SFDI of HC group, displayed on a binary logarithmic scale

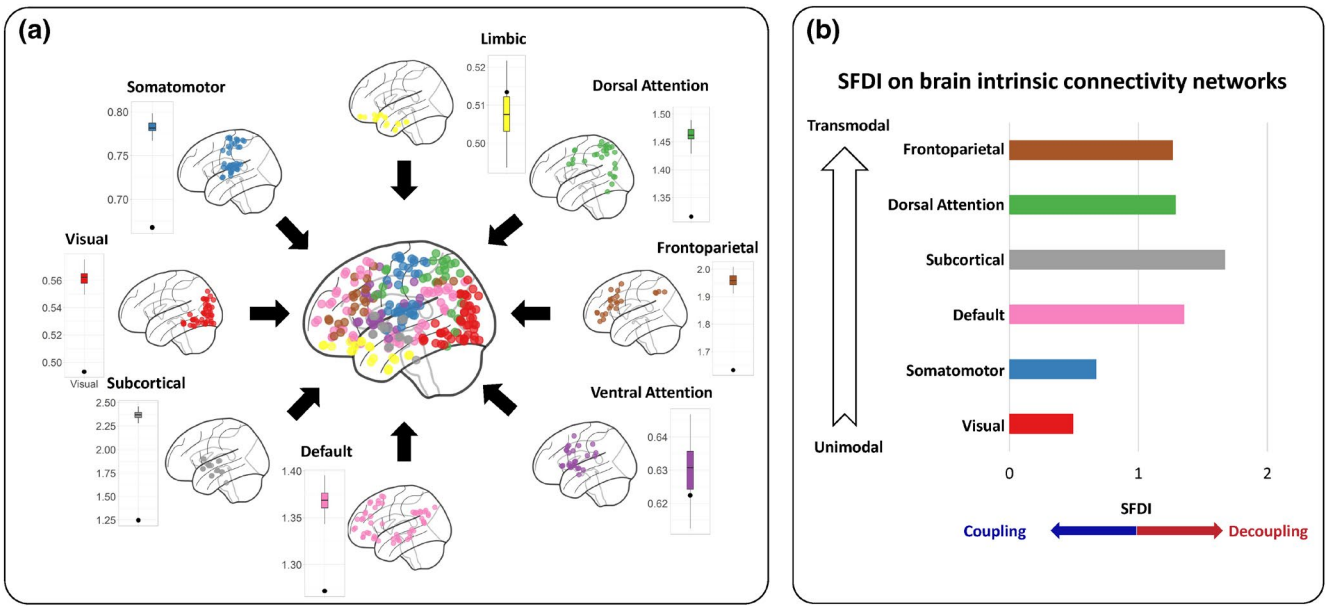

FIGURE 3 Null model results of the SFDI for each ICN obtained from the empirical/surrogate brain functional activity on HC group. (a) In each boxplot of the SFDI value, the box denotes null distribution from 100 randomization, while the black point denotes the empirical functional signals. (b) The rank of the SFDI for each significant ICN rejecting the null hypothesis

networks ($r = 0.43$, $p = 0.003$) in HC, indicating the interplay between SC and functional activity could be partially affected by the intrinsic connectivity strength, particularly on transmodal ICNs (see Figure S4).

3.5 | Group comparisons of decoupling index

In the GLM controlling for age, sex, and head motion, the SFDI of MS was significantly higher in the somatomotor network (T = 2.16, raw

TABLE 2 GLM examining the effects of the participant group, age, sex, and head motion on SFDI for all subjects

	HC vs. MS			Age			Sex			Head motion (mm)			Model statistics		
ICN SFDI	*β*	*T*	*p values*	*β*	*T*	*p values*	*β*	*T*	*p values*	*β*	*T*	*p values*	°	*F*	*p values*
Visual	−0.04	−2.67	**0.01**	−0.001	−1.34	0.18	−0.01	−0.64	0.52	−0.07	−0.56	0.58	108	7.85	**0.01**
Somatomotor	0.05	2.16	**0.03**	−0.001	−0.70	0.48	−0.02	−0.71	0.48	−0.15	−0.91	0.36	108	4.15	**0.04**
Dorsal attention	−0.12	−2.23	**0.03**	−0.008	−2.70	**0.01**	−0.07	−1.15	0.25	0.24	0.56	0.58	108	5.36	**0.02**
Frontoparietal	−0.01	−0.14	0.89	−0.004	−1.17	0.24	0.13	1.66	0.09	0.17	0.30	0.76	108	0.01	0.94
Default	−0.08	−1.88	0.06	−0.002	−1.07	0.29	−0.03	−0.64	0.52	0.23	0.76	0.45	108	3.71	0.06
Subcortical	−0.10	−2.32	**0.02**	−0.001	−0.39	0.70	−0.03	−0.73	0.47	−0.34	−1.01	0.317	108	6.03	**0.02**

Bold values indicates statistical significance at the $p < 0.05$ level.

$p = 0.03$, $p = 0.04$ with FDR correction), and significantly lower in the dorsal attention network (T = −2.23, raw $p = 0.03$, $p = 0.04$ with FDR correction), the subcortical network (T = −2.32, raw $p = 0.02$, $p = 0.04$ with FDR correction), and the visual network (T = −2.67, raw $p = 0.01$, $p = 0.04$ with FDR correction) compared with HC (see Table 2 and Figure 4). Similar structural-functional coupling trend was also observed on the default network (T = −1.88, raw $p = 0.06$). Significant age effect (T = −2.70, raw $p = 0.01$) was observed on SFDI variations only in the dorsal attention network. No sex or head motion effect was observed. The distribution of SFDI among CIS, RRMS, and HC groups was also visualized in Figure S5.

3.6 | Association between clinical phenotypes and decoupling index

When examining the effects of each brain ICN-level SFDI on disease duration or disease severity (EDSS), no significant clinical association was observed in MS patients. For imaging-cognition association, interestingly, we found SFDI in the somotomotor network was associated with lower PASAT-3 scale (beta = −24.31, T = −2.88, $p = 0.006$) in MS patients (F = 4.39, $p = 0.004$ for the linear model, see Figure 5 and Table 3). In consistent with the recent report (Koubiyr et al., 2021), our finding suggests that brain's incapacity to regulate functional activity in response to structural damage may represent a maladaptive process affecting cognitive performance in MS. The significant age effect was also observed on MS patient's cognitive function (beta = −0.37, T = −3.28, $p = 0.002$). In contrast, none of the FC graph metrics (global efficiency, clustering coefficient and network modularity) in the somatomotor network was correlated with PASAT-3 scale in MS (see Table S3), indicating superiority of SFDI measurements by stronger association with cognitive worsening.

4 | DISCUSSION

This is the first study to investigate MS neuropathology from the perspective of brain structural-functional coupling using GFA approach. We showed that the structural-functional high-order interaction could be quantified as a single decoupling index, which serves as a trait-like feature among brain ICNs in HC. In CIS and RRMS, this structural-functional interaction aberrantly is decoupled in the somatomotor network, and coupled in the visual, dorsal attention, and subcortical networks. These findings, along with the observed correlation between SFDI variations and cognitive function in MS, suggest the important role of brain structural-functional coupling mechanism underlying MS evolution.

By introducing SFDI, we demonstrated that two distinct spatial patterns emerged in healthy brains (Figure 3). Specifically, the functional activities in the somatomotor and visual networks were more rigidly constrained by the structural wiring (SFDI < 1), while the functional activity particularly in the dorsal attention, frontoparietal, default, and subcortical networks deviated from the structural

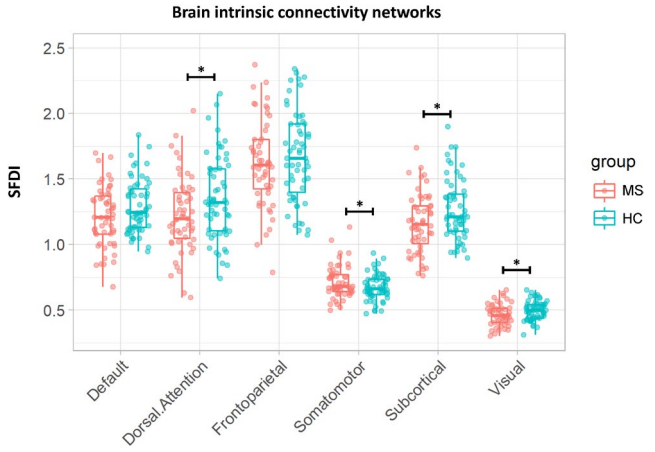

FIGURE 4 Box–whisker plot of brain ICN-level SFDI for HC and MS. The two whiskers extend from the first quartile to the smallest value and from the third quartile to the largest value. The median is shown with a bold line. $^{*}p < 0.05$; $^{**}p < 0.01$; $^{***}p < 0.001$

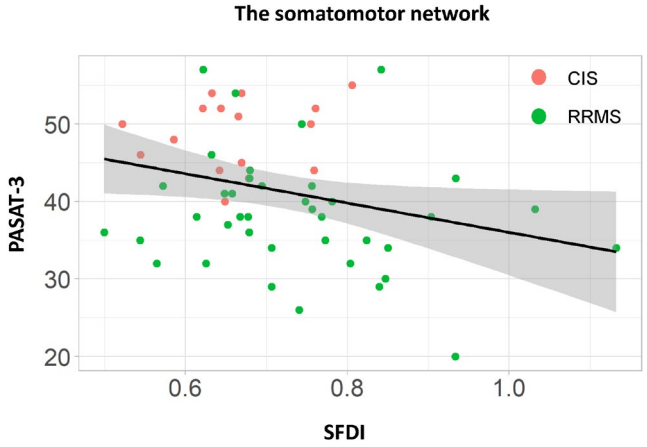

FIGURE 5 Correlation plot between SFDI on the somatomotor network and PASAT-3 scale for MS, where each green ball denotes a RRMS patient and each red ball denotes a CIS patient

wiring (SFDI > 1). Consistently, the structural-functional alignment was more associated with lower-level brain function (or unimodal functional area), and the opposite was true for higher-level brain function (or transmodal functional area) (Preti & Van De Ville 2019; Vazquez-Rodriguez et al., 2019). We suggest this spatial pattern probably reflect the intrinsic brain gradient, which was recently revealed from cortical microstructure (Huntenburg et al., 2017), temporal hierarchy (Chaudhuri et al., 2015), and functional connectivity (Margulies et al., 2016). Although the mechanism underlying this structural-functional coupling manifestation needs further exploration, one intuitive related interpretation is that reliable and fast task processing within unimodal areas may require a higher structural-functional coupling, whereas decoupled ICNs allow more flexible and complex processing in transmodal emotional and cognitive tasks.

Our results revealed a wide-spread rearrangement of brain structural-functional interplay in CIS and RRMS. This aberrant effect,

TABLE 3 GLM examining the effects of the somatomotor network SFDI, age, sex, and head motion on PASAT-3 scale for all MS patients

	Somatomotor SFDI			Age			Sex			Head motion (mm)			Model statistics		
	β	*T*	*p value*	*β*	*T*	*p value*	*β*	*T*	*p value*	*β*	*T*	*p value*	°	*F*	*p value*
PASAT-3	−24.31	−2.88	**0.006**	−0.37	−3.28	**0.002**	−0.39	−0.18	0.86	−16.26	−1.06	0.30	50	4.39	**0.004**

Bold values indicates statistical significance at the $p < 0.05$ level.

particularly observed in the somatomotor, visual, subcortical, and dorsal attention (also known as salience) networks, resonates with previous neuropathological evidences. Consistently, Koubiyr et al. observed structural-functional decoupling changes in the visual, somatomotor, and salience networks after 1 year following CIS onset (Koubiyr et al., 2019), and inversely coupled on the whole-brain level after 5 years following CIS onset (Koubiyr et al., 2021). Such complex structural-functional coupling and decoupling effects were also been seen in neuropathological disorders including schizophrenia (Cocchi et al., 2014; Skudlarski et al., 2010), bipolar disorder (Zhang et al., 2019), idiopathic generalized epilepsy (Zhang et al., 2011), and psychogenic nonepileptic seizures (Ding et al., 2013). From our observations, the tight structural-functional coupling in the somatomotor network was decreased in MS, indicating of weaker constraint of the underlying wiring diagram impart on brain activity. On the other hand, greater anatomical constraints in the visual, subcortical, and dorsal attention networks suggested a damaged capacity of the brain to reconfigure neuronal signaling in MS.

Moreover, the structural-functional coupling degree in the somatomotor network can predict the cognitive function in MS (see Table 3). To put it into perspective, 0.1 unit increase in SFDI in the somatomotor network was equivalent to 2.4 points cognitive decline in PASAT-3 scale. As one prominent ICN exhibiting functional disconnection in MS (Tahedl et al., 2018), we argue that the somatomotor network with excessive decoupling structural-functional interplay may play a maladaptive role in cognitive worsening of MS patients. Our evidence supports the hypothesis that cognition relevant changes could be induced by complex neural dynamics result from structural disconnection. Inconsistently, Hellyer et al revealed that decreased metastable neural dynamics disrupted by structural disconnection were associated with reduced cognitive flexibility and information processing (Hellyer et al., 2015). We suspect that the association between cognitive decline and the aberrantly stronger structural-functional coupling may be explained by disordered internal neuromechanism such as homeostatic plasticity (Rocha et al., 2018; Turrigiano, 2011). Interestingly, we did not find any cognition-relevant association with coupling variations on the default mode network, which was traditionally considered as a hallmark network in MS. This could be attributed to different spatial scales and metrics (FC vs. coupling). The previously reported altered brain FC related to a worsen performance in MS was almost referred to inter-areal connectivity within the default mode network (Eijlers et al., 2017; Louapre et al., 2014), whereas the structural-functional coupling was averaged for each ICN in our analysis.

A related question is which factor contributes to MS-related structural-functional coupling rearrangement. When examining the underlying physiological factors, we observed that none of age, sex, or head motion during scanning was associated with brain structural-functional interaction. Inconsistently, brain structural-functional coupling was found to exhibit slightly stronger in older males (Gu et al., 2021). We postulate this inconsistency may be attributable to the coupling definition difference (SC-FC correlation vs. SFDI). Furthermore, the variation of brain FC network topology was not only uncorrelated with ICN-level SFDI, but also exhibited no disturbance effects in the SFDI-cognition association in MS cohort. Therefore, we argue that SFDI is an important imaging indicator to detect neuropathology of MS, independent of functional network topology. More evidence from molecular neuropathological studies is further needed to validate the exact mechanism of structural-functional coupling signature related to MS.

We acknowledge that our study is not without limitations. First, the optimal fiber tracking method in structural brain network construction is still controversial, for regions with more frequent fiber disposition are more likely to obtain potential errors during fiber tract reconstruction. To maximally avoid such effects, the anatomical-constrained tractography method for tractography estimation with anatomical priors was performed to improve the biological plausibility of the generated streamlines (Smith et al., 2012). Second, the current study only includes early stage (CIS) and relapsing-remitting stage of MS patients. Future studies can investigate the primary progressive stage to explicitly unveil whether the brain coupling signatures in different periods constitute a continuum. Besides, the sample size in our cross-sectional study is relatively small, especially for CIS patients. Validation of the observed MS-associated brain structural-functional coupling requires further longitudinal examinations on larger cohorts. Finally, more comprehensive neurological examinations such as Minimal Assessment of Cognitive Function in Multiple Sclerosis (MACFIMS) are needed to validate the exact role of SFDI changes in MS cognitive worsening.

In summary, this study provides a new avenue to quantitatively delineate the brain structural-functional association variation affected by MS in the GFA framework. The excessive reorganization of brain structural-functional interplay on the visual, somatomotor, dorsal attention and subcortical networks was identified in MS. Furthermore, this structural-functional coupling exhibited on the somatomotor network in MS associates with cognitive worsening. Overall, our study suggests a unique signature of brain structural-functional reorganization in MS.

DECLARATION OF TRANSPARENCY

The authors, reviewers and editors affirm that in accordance to the policies set by the *Journal of Neuroscience Research*, this manuscript presents an accurate and transparent account of the study being reported and that all critical details describing the methods and results are present.

ACKNOWLEDGMENTS

We thank Dr. Susumu Mori for the consultation of the brain intrinsic connectivity networks defined in our data analysis. We thank Dr. Bowen Xin for manuscript revision. We also acknowledge Mindsgo Life Science Shenzhen Co. Ltd for technical support on image data management on BrainLabel cloud platform http://brainlabel.org/.

CONFLICT OF INTEREST

The authors (C Ye, J Huang, L Liang, Z Yan, Z Qi, X Kang, Z Liu, H Dong, H Lv, T Ma, and J Lu) declare no competing interests.

AUTHOR CONTRIBUTIONS

Chenfei Ye: Methodology (lead); Writing – Original Draft Preparation (equal). Jing Huang: Writing – Original Draft Preparation (equal). Liang Li: Validation. Zehong Yan: Data Curation. Zhigang Qi: Resources (equal). Xiong Kang: Resources (equal). Zheng Liu: Resources (equal). Huiqing Dong: Resources (equal). Haiyan Lv: Software. Jie Lu: Funding Acquisition; Supervision (equal). Ting Ma: Project Administration; Supervision (equal); Writing – review and editing.

PEER REVIEW

The peer review history for this article is available at https://publons.com/publon/10.1002/jnr.25028.

DATA AND CODE AVAILABILITY

The data that support the findings of this study are available on request from the corresponding author. The data are not publicly available due to privacy or ethical restrictions. Multimodal MR image processing was performed in Python. GFA was conducted in python using the pygsp library (https://pypi.org/project/pygsp/). Statistical analyses were performed in R. Code for all analyses and visualizations is being made available online through https://github.com/figo2150/graph_freq_MS/.

REFERENCES

Atasoy, S., Deco, G., Kringelbach, M. L., & Pearson, J. (2018). Harmonic brain modes: A unifying framework for linking space and time in brain dynamics. *Neuroscientist*, *24*, 277–293.

Atasoy, S., Donnelly, I., & Pearson, J. (2016). Human brain networks function in connectome-specific harmonic waves. *Nature Communications*, *7*, 10340.

Avants, B. B., Epstein, C. L., Grossman, M., & Gee, J. C. (2008). Symmetric diffeomorphic image registration with cross-correlation: Evaluating automated labeling of elderly and neurodegenerative brain. *Medical Image Analysis*, *12*, 26–41.

Bassett, D. S., & Sporns, O. (2017). Network neuroscience. *Nature Neuroscience*, *20*, 353–364.

Battaglini, M., Jenkinson, M., & De Stefano, N. (2012). Evaluating and reducing the impact of white matter lesions on brain volume measurements. *Human Brain Mapping*, *33*, 2062–2071.

Bisecco, A., Altieri, M., Santangelo, G., Di Nardo, F., Docimo, R., Caiazzo, G., Capuano, R., Pappacena, S., d'Ambrosio, A., Bonavita, S., Trojsi, F., Cirillo, M., Esposito, F., Tedeschi, G., & Gallo, A. (2019). Resting-state functional correlates of social cognition in multiple sclerosis: An explorative study. *Frontiers in Behavioral Neuroscience*, *13*, 276.

Calabrese, M., Magliozzi, R., Ciccarelli, O., Geurts, J. J., Reynolds, R., & Martin, R. (2015). Exploring the origins of grey matter damage in multiple sclerosis. *Nature Reviews Neuroscience*, *16*, 147–158.

Charalambous, T., Tur, C., Prados, F., Kanber, B., Chard, D. T., Ourselin, S., Clayden, J. D., Wheeler-Kingshott, C. A. G., Thompson, A. J., & Toosy, A. T. (2019). Structural network disruption markers explain disability in multiple sclerosis. *Journal of Neurology, Neurosurgery, and Psychiatry*, *90*, 219–226.

Chaudhuri, R., Knoblauch, K., Gariel, M. A., Kennedy, H., & Wang, X. J. (2015). A Large-Scale Circuit Mechanism for Hierarchical Dynamical Processing in the Primate Cortex. *Neuron*, *88*, 419–431.

Ciric, R., Wolf, D. H., Power, J. D., Roalf, D. R., Baum, G. L., Ruparel, K., Shinohara, R. T., Elliott, M. A., Eickhoff, S. B., Davatzikos, C., Gur, R. C., Gur, R. E., Bassett, D. S., & Satterthwaite, T. D. (2017). Benchmarking of participant-level confound regression strategies for the control of motion artifact in studies of functional connectivity. *Neuroimage*, *154*, 174–187.

Cocchi, L., Harding, I. H., Lord, A., Pantelis, C., Yucel, M., & Zalesky, A. (2014). Disruption of structure-function coupling in the schizophrenia connectome. *Neuroimage Clinical*, *4*, 779–787.

Cox, R. W. (1996). AFNI: Software for analysis and visualization of functional magnetic resonance neuroimages. *Computers and Biomedical Research*, *29*, 162–173.

Cui, F., Zhou, L., Wang, Z., Lang, C., Park, J., Tan, Z., Yu, Y., Sun, C., Gao, Y., & Kong, J. (2017). Altered functional connectivity of striatal subregions in patients with multiple sclerosis. *Frontiers in Neurology*, *8*, 129.

Ding, J. R., An, D., Liao, W., Li, J., Wu, G. R., Xu, Q., Long, Z., Gong, Q., Zhou, D., Sporns, O., & Chen, H. (2013). Altered functional and structural connectivity networks in psychogenic non-epileptic seizures. *PLoS ONE*, *8*, e63850.

Eijlers, A. J., Meijer, K. A., Wassenaar, T. M., Steenwijk, M. D., Uitdehaag, B. M., Barkhof, F., Wink, A. M., Geurts, J. J., & Schoonheim, M. M. (2017). Increased default-mode network centrality in cognitively impaired multiple sclerosis patients. *Neurology*, *88*, 952–960.

Esteban, O., Markiewicz, C. J., Blair, R. W., Moodie, C. A., Isik, A. I., Erramuzpe, A., Kent, J. D., Goncalves, M., DuPre, E., Snyder, M., Oya, H., Ghosh, S. S., Wright, J., Durnez, J., Poldrack, R. A., & Gorgolewski, K. J. (2019). fMRIPrep: A robust preprocessing pipeline for functional MRI. *Nature Methods*, *16*, 111–116.

Filippi, M., Bar-Or, A., Piehl, F., Preziosa, P., Solari, A., Vukusic, S., & Rocca, M. A. (2018). Multiple sclerosis. *Nature Reviews Disease Primers*, *4*, 43.

Fischl, B. (2012). FreeSurfer. *Neuroimage*, *62*, 774–781.

Friston, K. J., Williams, S., Howard, R., Frackowiak, R. S., & Turner, R. (1996). Movement-related effects in fMRI time-series. *Magnetic Resonance in Medicine*, *35*, 346–355.

Glasser, M. F., Coalson, T. S., Robinson, E. C., Hacker, C. D., Harwell, J., Yacoub, E., Ugurbil, K., Andersson, J., Beckmann, C. F., Jenkinson, M., Smith, S. M., & Van Essen, D. C. (2016). A multi-modal parcellation of human cerebral cortex. *Nature*, *536*, 171–178.

Greve, D. N., & Fischl, B. (2009). Accurate and robust brain image alignment using boundary-based registration. *Neuroimage*, *48*, 63–72.

Gu, Z., Jamison, K. W., Sabuncu, M. R., & Kuceyeski, A. (2021). Heritability and interindividual variability of regional structure-function coupling. *Nature Communications*, *12*, 4894.

Hagmann, P., Kurant, M., Gigandet, X., Thiran, P., Wedeen, V. J., Meuli, R., & Thiran, J. P. (2007). Mapping human whole-brain structural networks with diffusion MRI. *PLoS ONE*, *2*, e597.

Hellyer, P. J., Scott, G., Shanahan, M., Sharp, D. J., & Leech, R. (2015). Cognitive flexibility through metastable neural dynamics is disrupted by damage to the structural connectome. *Journal of Neuroscience*, *35*, 9050–9063.

Honey, C. J., Sporns, O., Cammoun, L., Gigandet, X., Thiran, J. P., Meuli, R., & Hagmann, P. (2009). Predicting human resting-state functional connectivity from structural connectivity. *Proceedings of the National Academy of Sciences of the United States of America*, *106*, 2035–2040.

Horbruegger, M., Loewe, K., Kaufmann, J., Wagner, M., Schippling, S., Pawlitzki, M., & Schoenfeld, M. A. (2019). Anatomically constrained tractography facilitates biologically plausible fiber reconstruction of the optic radiation in multiple sclerosis. *Neuroimage Clinical*, *22*, 101740.

Huang, W., Goldsberry, L., Wymbs, N. F., Grafton, S. T., Bassett, D. S., & Ribeiro, A. (2016). Graph frequency analysis of brain signals. *IEEE Journal on Selected Topics in Signal Processing*, *10*, 1189–1203.

Huntenburg, J. M., Bazin, P. L., Goulas, A., Tardif, C. L., Villringer, A., & Margulies, D. S. (2017). A systematic relationship between functional connectivity and intracortical myelin in the human cerebral cortex. *Cerebral Cortex*, *27*, 981–997.

Jenkinson, M., Bannister, P., Brady, M., & Smith, S. (2002). Improved optimization for the robust and accurate linear registration and motion correction of brain images. *Neuroimage*, *17*, 825–841.

Koubiyr, I., Besson, P., Deloire, M., Charre-Morin, J., Saubusse, A., Tourdias, T., Brochet, B., & Ruet, A. (2019). Dynamic modular-level alterations of structural-functional coupling in clinically isolated syndrome. *Brain*, *142*, 3428–3439.

Koubiyr, I., Deloire, M., Brochet, B., Besson, P., Charre-Morin, J., Saubusse, A., Tourdias, T., & Ruet, A. (2021). Structural constraints of functional connectivity drive cognitive impairment in the early stages of multiple sclerosis. *Multiple Sclerosis*, *27*, 559–567.

Kurtzke, J. F. (1983). Rating neurologic impairment in multiple sclerosis: An expanded disability status scale (EDSS). *Neurology*, *33*, 1444–1452.

Liu, Y., Dai, Z., Duan, Y., Huang, J., Ren, Z., Liu, Z., Dong, H., Shu, N., Vrenken, H., Wattjes, M. P., Barkhof, F., He, Y., & Li, K. (2016). Whole brain functional connectivity in clinically isolated syndrome without conventional brain MRI lesions. *European Radiology*, *26*, 2982–2991.

Louapre, C., Perlbarg, V., Garcia-Lorenzo, D., Urbanski, M., Benali, H., Assouad, R., Galanaud, D., Freeman, L., Bodini, B., Papeix, C., Tourbah, A., Lubetzki, C., Lehericy, S., & Stankoff, B. (2014). Brain networks disconnection in early multiple sclerosis cognitive deficits: An anatomofunctional study. *Human Brain Mapping*, *35*, 4706–4717.

Margulies, D. S., Ghosh, S. S., Goulas, A., Falkiewicz, M., Huntenburg, J. M., Langs, G., Bezgin, G., Eickhoff, S. B., Castellanos, F. X., Petrides, M., Jefferies, E., & Smallwood, J. (2016). Situating the default-mode network along a principal gradient of macroscale cortical organization. *Proceedings of the National Academy of Sciences of the United States of America*, *113*, 12574–12579.

McCarthy, C. S., Ramprashad, A., Thompson, C., Botti, J. A., Coman, I. L., & Kates, W. R. (2015). A comparison of FreeSurfer-generated data with and without manual intervention. *Front Neurosci*, *9*, 379. https://doi.org/10.3389/fnins.2015.00379

Miller, D. H., Chard, D. T., & Ciccarelli, O. (2012). Clinically isolated syndromes. *Lancet Neurology*, *11*, 157–169.

Patenaude, B., Smith, S. M., Kennedy, D. N., & Jenkinson, M. (2011). A Bayesian model of shape and appearance for subcortical brain segmentation. *Neuroimage*, *56*, 907–922.

Pirondini, E., Vybornova, A., Coscia, M., & Van De Ville, D. (2016). A spectral method for generating surrogate graph signals. *IEEE Signal Processing Letters*, *23*, 1275–1278.

Polman, C. H., Reingold, S. C., Banwell, B., Clanet, M., Cohen, J. A., Filippi, M., Fujihara, K., Havrdova, E., Hutchinson, M., Kappos, L., Lublin, F. D., Montalban, X., O'Connor, P., Sandberg-Wollheim, M., Thompson, A. J., Waubant, E., Weinshenker, B., & Wolinsky, J. S. (2011). Diagnostic criteria for multiple sclerosis: 2010 revisions to the McDonald criteria. *Annals of Neurology*, *69*, 292–302.

Preti, M. G., & Van De Ville, D. (2019). Decoupling of brain function from structure reveals regional behavioral specialization in humans. *Nature Communications*, *10*, 4747.

Rocca, M. A., De Meo, E., & Filippi, M. (2016). Functional MRI in investigating cognitive impairment in multiple sclerosis. *Acta Neurologica Scandinavica*, *134*(Suppl 200), 39–46.

Rocha, R. P., Kocillari, L., Suweis, S., Corbetta, M., & Maritan, A. (2018). Homeostatic plasticity and emergence of functional networks in a whole-brain model at criticality. *Scientific Reports*, *8*, 15682.

Sbardella, E., Upadhyay, N., Tona, F., Prosperini, L., De Giglio, L., Petsas, N., Pozzilli, C., & Pantano, P. (2017). Dentate nucleus connectivity in adult patients with multiple sclerosis: Functional changes at rest and correlation with clinical features. *Multiple Sclerosis*, *23*, 546–555.

Schoonheim, M. M., Geurts, J., Wiebenga, O. T., De Munck, J. C., Polman, C. H., Stam, C. J., Barkhof, F., & Wink, A. M. (2014). Changes in functional network centrality underlie cognitive dysfunction and physical disability in multiple sclerosis. *Multiple Sclerosis*, *20*, 1058–1065.

Shu, N., Duan, Y., Huang, J., Ren, Z., Liu, Z., Dong, H., Barkhof, F., Li, K., & Liu, Y. (2018). Progressive brain rich-club network disruption from clinically isolated syndrome towards multiple sclerosis. *Neuroimage Clinical*, *19*, 232–239.

Skudlarski, P., Jagannathan, K., Anderson, K., Stevens, M. C., Calhoun, V. D., Skudlarska, B. A., & Pearlson, G. (2010). Brain connectivity is not only lower but different in schizophrenia: A combined anatomical and functional approach. *Biological Psychiatry*, *68*, 61–69.

Smith, R. E., Tournier, J. D., Calamante, F., & Connelly, A. (2012). Anatomically-constrained tractography: Improved diffusion MRI streamlines tractography through effective use of anatomical information. *Neuroimage*, *62*, 1924–1938.

Smith, R. E., Tournier, J. D., Calamante, F., & Connelly, A. (2015). The effects of SIFT on the reproducibility and biological accuracy of the structural connectome. *Neuroimage*, *104*, 253–265.

Solana, E., Martinez-Heras, E., Martinez-Lapiscina, E. H., Sepulveda, M., Sola-Valls, N., Bargallo, N., Berenguer, J., Blanco, Y., Andorra, M., Pulido-Valdeolivas, I., Zubizarreta, I., Saiz, A., & Llufriu, S. (2018). Magnetic resonance markers of tissue damage related to connectivity disruption in multiple sclerosis. *Neuroimage Clinical*, *20*, 161–168.

Sporns, O. (2011). The human connectome: A complex network. *Annals of the New York Academy of Sciences*, *1224*, 109–125.

Stiso, J., & Bassett, D. S. (2018). Spatial Embedding Imposes Constraints on Neuronal Network Architectures. *Trends in Cognitive Sciences*, *22*, 1127–1142.

Suarez, L. E., Markello, R. D., Betzel, R. F., & Misic, B. (2020). Linking structure and function in macroscale brain networks. *Trends in Cognitive Sciences*, *24*, 302–315.

Tahedl, M., Levine, S. M., Greenlee, M. W., Weissert, R., & Schwarzbach, J. V. (2018). Functional connectivity in multiple sclerosis: Recent findings and future directions. *Frontiers in Neurology*, *9*, 828.

Tillema, J. M., Hulst, H. E., Rocca, M. A., Vrenken, H., Steenwijk, M. D., Damjanovic, D., Enzinger, C., Ropele, S., Tedeschi, G., Gallo, A., Ciccarelli, O., Rovira, A., Montalban, X., de Stefano, N., Stromillo, M. L., Filippi, M., Barkhof, F., & MAGNIMS Study Group. (2016). Regional cortical thinning in multiple sclerosis and its relation with cognitive impairment: A multicenter study. *Multiple Sclerosis*, *22*, 901–909.

Tinelli, E., Francia, A., Quartuccio, E. M., Morreale, M., Contessa, G. M., Pascucci, S., Sbardella, E., Pozzilli, C., & Pantano, P. (2013). Structural brain MR imaging changes associated with obsessive-compulsive disorder in patients with multiple sclerosis. *American Journal of Neuroradiology*, *34*, 305–309.

Tournier, J. D., Calamante, F., & Connelly, A. (Eds.). (2010). Improved probabilistic streamlines tractography by 2nd order integration over fibre orientation distributions. In *Proceedings of the International Society for Magnetic Resonance in Medicine*, Ismrm, p. 1670.

Tournier, J. D., Calamante, F., & Connelly, A. (2012). MRtrix: Diffusion tractography in crossing fiber regions. *International Journal of Imaging Systems and Technology*, *22*, 53–66.

Tournier, J. D., Yeh, C. H., Calamante, F., Cho, K. H., Connelly, A., & Lin, C. P. (2008). Resolving crossing fibres using constrained spherical deconvolution: Validation using diffusion-weighted imaging phantom data. *Neuroimage*, *42*, 617–625.

Tur, C., Grussu, F., Prados, F., Charalambous, T., Collorone, S., Kanber, B., Cawley, N., Altmann, D. R., Ourselin, S., Barkhof, F., Clayden, J. D.,

Toosy, A. T., Wheeler-Kingshott, C. A. G., & Ciccarelli, O. (2019). A multi-shell multi-tissue diffusion study of brain connectivity in early multiple sclerosis. *Multiple Sclerosis*, *26*, 774–785.

Turrigiano, G. (2011). Too many cooks? Intrinsic and synaptic homeostatic mechanisms in cortical circuit refinement. *Annual Review of Neuroscience*, *34*, 89–103.

Vazquez-Rodriguez, B., Suarez, L. E., Markello, R. D., Shafiei, G., Paquola, C., Hagmann, P., van den Heuvel, M. P., Bernhardt, B. C., Spreng, R. N., & Misic, B. (2019). Gradients of structure-function tethering across neocortex. *Proceedings of the National Academy of Sciences of the United States of America*, *116*, 21219–21227.

Wang, Z., Dai, Z., Gong, G., Zhou, C., & He, Y. (2015). Understanding structural-functional relationships in the human brain: A large-scale network perspective. *Neuroscientist*, *21*, 290–305.

Yeo, B. T., Krienen, F. M., Sepulcre, J., Sabuncu, M. R., Lashkari, D., Hollinshead, M., Roffman, J. L., Smoller, J. W., Zollei, L., Polimeni, J. R., Fischl, B., Liu, H., & Buckner, R. L. (2011). The organization of the human cerebral cortex estimated by intrinsic functional connectivity. *Journal of Neurophysiology*, *106*, 1125–1165.

Zhang, J., Cortese, R., De Stefano, N., & Giorgio, A. (2021). Structural and functional connectivity substrates of cognitive impairment in multiple sclerosis. *Frontiers in Neurology*, *12*, 671894.

Zhang, R., Shao, R., Xu, G., Lu, W., Zheng, W., Miao, Q., Chen, K., Gao, Y., Bi, Y., Guan, L., McIntyre, R. S., Deng, Y., Huang, X., So, K. F., & Lin, K. (2019). Aberrant brain structural-functional connectivity coupling in euthymic bipolar disorder. *Human Brain Mapping*, *40*, 3452–3463.

Zhang, Z., Liao, W., Chen, H., Mantini, D., Ding, J. R., Xu, Q., Wang, Z., Yuan, C., Chen, G., Jiao, Q., & Lu, G. (2011). Altered functional-structural coupling of large-scale brain networks in idiopathic generalized epilepsy. *Brain*, *134*, 2912–2928.

Zipp, F., Gold, R., & Wiendl, H. (2013). Identification of inflammatory neuronal injury and prevention of neuronal damage in multiple sclerosis: Hope for novel therapies? *JAMA Neurology*, *70*, 1569–1574.

SUPPORTING INFORMATION

Additional supporting information may be found in the online version of the article at the publisher's website.

FIGURE S1 Flowchart of study population

FIGURE S2 The median-split cutoff splitting the BOLD power spectrum density (blue curve) was defined to decompose brain activity into coupled (light blue) and decoupled (light red) portions. The shaded band around the curve was calculated according to ± one standard deviation

FIGURE S3 Distribution of the sum of structural connectivity strength on brain ICNs for HC subjects

FIGURE S4 Correlation plot between the sum of structural connectivity strength and SFDI on each brain ICN for HC subjects. The partial correlation coefficients and the corresponding *p*-values adjusted by age and sex are also shown in each subplot

FIGURE S5 Box-whisker plot of SFDI of brain ICNs for HC, CIS and RRMS. The two whiskers extend from the first quartile to the smallest value and from the third quartile to the largest value. The median is shown with a bold line

TABLE S1 GLM examining the effects of the age, sex and head motion on SFDI of brain ICNs for HC

TABLE S2 Summary of Spearman correlations between the functional network graph metrics and SFDI of brain ICNs in HC and MS

TABLE S3 GLM examining the effects of the somatomotor functional network graph metrics, age, sex and head motion on PASAT-3 scale for all MS patients

Transparent Science Questionnaire for Authors

How to cite this article: Ye, C., Huang, J., Liang, L., Yan, Z., Qi, Z., Kang, X., Liu, Z., Dong, H., Lv, H., Ma, T. & Lu, J. (2022). Coupling of brain activity and structural network in multiple sclerosis: A graph frequency analysis study. *Journal of Neuroscience Research*, 100, 1226–1238. https://doi.org/10.1002/jnr.25028